JOURNAL OF SPACECRAFT AND ROCKETS
Vol. 46, No. 2, March–April 2009

Entry Trajectory Model with Thermomechanical Breakup

Ashish Tewari*
Indian Institute of Technology, Kanpur 208 016, India

DOI: 10.2514/1.39651

A procedure for modeling the entry trajectory with aerothermal breakup is presented, incorporating an accurate flow model and complete vehicle dynamics. The method accounts for thermomechanical breakup into multiple fragments due to evolving surface thermal gradients and centrifugal stresses using an empirical model that produces a most probable cutplane. The detailed geometric and inertial modules have been coded to generate fragments of a general shape and size. The iteration over debris fragments includes complete thermal ablation and mechanical disintegration by centrifugal stresses. As soon as new debris is generated, its state vector and geometry is fed back to the dynamics and aerothermal loads modules, and simulation is performed over the next time interval. Only the largest surviving fragment is tracked for long-term simulation, whereas the other fragments are tracked for a prespecified duration. When a fragment is either completely ablated/disintegrated or reaches ground level, its simulation is ended. Hence, the scheme results in a complete simulation of the entry trajectory with en route debris shedding events until either ground impact or complete ablation and mechanical disintegration. Sample trajectory simulations for an entry capsule representative of deboost from a circular (or elliptical) orbit are considered. A dispersion analysis based on variations in the entry conditions has been conducted and its effect on the probable debris field is calculated. The speed and flight-path angle have the largest effect on downrange dispersion, whereas the heading angle affects cross-range dispersion the most. Increase in the object's entry mass (assumed nominally distributed) has a negligible effect on the debris field, whereas a 10% decrease in the mass causes an appreciable variation in debris dispersion.

Nomenclature

A	=	reference area
a_N	=	centrifugal acceleration magnitude
a_R	=	reference centrifugal acceleration magnitude
C_p	=	pressure coefficient
C_τ	=	shear stress coefficient
c	=	reference length
c_p	=	constant pressure specific heat
D	=	drag
F_y	=	side force
$\mathbf{f}$	=	external force vector, $\mathbf{f} \in \Re^{3\times 1} = (-D, L, F_y)^T$
G_i	=	thermomechanical stress parameter for the ith surface panel
g_R, g_ϕ	=	radial and tangential components of acceleration due to gravity ($g = g_R$, $g_\phi = 0$ for spherical model)
h	=	geometric altitude
h_w, h_{aw}	=	static enthalpy at wall, static enthalpy at adiabatic wall
h_0	=	total enthalpy
$\mathbf{J}$	=	inertia tensor, $\mathbf{J} \in \Re^{3\times 3}$
J_{11}, J_{22}, J_{33}	=	principal moments of inertia
J_2, J_3, J_4	=	Jeffrey's constants
Kn	=	Knudsen number
L	=	lift
M	=	Mach number
m	=	mass of the body
$\hat{\mathbf{n}}_i$	=	unit normal vector of the ith surface panel
Pr	=	Prandtl number
p_∞	=	freestream static pressure
p, q, r	=	angular velocity components about the principal axes
$\dot{Q}$	=	convective heat flux on the ith surface panel
$\dot{Q}_R$	=	reference convective heat flux
q_∞	=	freestream dynamic pressure
q_0, q_1, q_2, q_3	=	quaternion components used to describe body orientation
R	=	distance of center of mass from Earth's center
r_n	=	radius of spherical stagnation region (nose radius)
$\mathbf{S}(\boldsymbol{\omega})$	=	skew symmetric matrix, $\mathbf{S}(\boldsymbol{\omega}) \in \Re^{3\times 3}$
s	=	molecular speed ratio, $s = V/c'$, where c' is the most probable thermal speed of atmospheric particles
T_0	=	total temperature
T_w	=	wall static temperature
T_∞	=	static pressure temperature
u_e	=	tangential flow speed at the edge of boundary layer
V	=	speed measured in the planet fixed coordinate system (airspeed)
$\mathbf{v}_i$	=	effective flow velocity at centroid of the ith panel
$\hat{\mathbf{v}}_i$	=	$\mathbf{v}_i/\lvert\mathbf{v}_i\rvert$
$\mathbf{v}_\infty$	=	freestream velocity vector
χ	=	heading angle, measured clockwise from north
x	=	distance along the edge of the boundary layer
γ	=	flight-path angle, positive above the local horizon
$\tilde{\gamma}$	=	specific heat ratio of air, taken as 1.4
δ	=	latitude, positive above equator
Θ	=	inclination of an elemental panel with respect to flow direction, $\hat{\mathbf{v}}_i$
λ	=	longitude, positive toward east
μ_e	=	dynamic viscosity coefficient at the edge of boundary layer
ρ_∞	=	freestream density
$\boldsymbol{\rho}_i$	=	position vector of ith panel centroid from center of mass
$\boldsymbol{\tau}$	=	external moment vector, $\boldsymbol{\tau} \in \Re^{3\times 1}$
Ω	=	rotational rate of Earth

Received 8 July 2008; revision received 14 January 2009; accepted for publication 14 January 2009.

*Professor, Department of Aerospace Engineering; ashtew@iitk.ac.in. Senior Member AIAA.

$\boldsymbol{\omega}$ = angular velocity vector of the body, $\boldsymbol{\omega} \in \Re^{3\times 1}$

Subscript

e = quantities at boundary-layer edge

Superscript

$\cdot$ = time derivative

Introduction

SPACE debris entry simulation and impact estimates form a topic of active research with several practical applications [1–6]. Every launch and recovery mission must not only carefully account for likely debris fields to be encountered, but also predict the likely impact points of spent stages and deorbited satellites after atmospheric entry. Modeling the breakup of an entering object based on aerothermal loads is an important (albeit difficult) task of space debris researchers. Several rough and ready methods have been proposed, either to account for a predefined debris field in space or to analyze that created by explosive events, which then enters the atmosphere, falling in a specific region. Lips et al. [5], in their SCARAB code, present a 6 degree-of-freedom simulation strategy for predicting thermal and mechanical fragmentation. Thermal fragmentation is produced by chains of molten volume panels that destroy the connectivity between vehicle components. Mechanical fragmentation due to aerodynamic and inertia loads is restricted to predetermined cutplanes, where a detailed stress analysis with temperature-dependent material data is conducted. Lips et al. [6] compare the demise results of [5] for some simple shapes with those of a NASA code called ORSAT, which is based on a 3 degree-of-freedom simulation. The ORSAT code treats the entry body as a set of simple objects covered by a container. Upon melting of the container, the internal objects are released and tracked until thermal melting or ground impact. Using secondary containers, multiple fragmentations can also be modeled.

The present work aims to model debris entry trajectory with thermomechanical fragmentation due to evolving cutplanes, based on heat flux and centrifugal acceleration. For modeling the entry trajectory, a self-contained aerothermal model and complete 6 degree-of-freedom body dynamics are employed in an Earth-fixed rotating frame, with detailed standard atmosphere and oblate gravity models. The kinematical and dynamic equations of motion in terms of latitude, longitude, altitude, velocity, flight-path inclination, heading angle, attitude angles, and body rates have been integrated in time to yield trajectory with initial conditions in each phase. The aerodynamic forces, moments, and heat flux are calculated as functions of body attitude, velocity, and altitude. A local surface inclination panel method is used employing either a Maxwellian velocity distribution for free-molecular flow, a modified Newtonian/boundary-layer approximation for continuum hypersonic flow, or a Kn-based bridging relation [7] for the transition regime. A spatial integration of the loads over all the panels is then performed to yield total vehicle loads. The use of this approach makes the trajectory model more accurate and the simulation more realistic than the traditional method of employing tabular aerothermodynamic data into a flight mechanics module.

The main thrust of the present paper is to propose a logical scheme for debris generation by atmospheric entry based on thermal flux and centrifugal acceleration patterns on the object surface, thereby producing a most probable cutplane. The detailed geometric and inertial modules can then be programmed to generate fragments of a general shape and size. Such a method has the advantage of being flexible in terms of using the limiting heat flux and load factors, separately obtained by material and structural considerations. A detailed trajectory and aerothermal model can then be combined with the prediction of breakup and fragmentation events.

Entry Dynamics and Trajectory Simulation

To accurately model the dynamics of atmospheric debris, one must employ an aerothermal model appropriate for entry from a general orbital state, as well as simulate the motion of an arbitrarily shaped object with complete rigid-body kinematics and kinetics. Boldface symbols represent either vectors (lowercase) or matrices (uppercase). The starred quantities represent variables in the inertial frame.

Dynamic Model

The Earth-centered, nonrotating frame is taken as the inertial reference coordinate system. The equations of motion for the atmospheric phase are developed in the local horizon relative to an Earth-fixed geocentric frame, rotating with the planet [8]. The aerodynamic model calculates forces and moments with respect to the body-fixed axes and transforms them to the local horizon frame. The kinematical equations of particle motion are as follows:

$$\dot{\lambda} = \frac{V\cos\gamma\sin\chi}{R\cos\delta} \tag{1}$$

$$\dot{\delta} = \frac{V\cos\gamma\cos\chi}{R} \tag{2}$$

$$\dot{R} = V\sin\gamma \tag{3}$$

The kinetic equations of particle motion can be written as follows [8]:

$$\dot{V} = -g_R\sin\gamma + g_\phi\cos\gamma\cos\chi - \frac{D}{m} + \Omega^2 R\cos\delta(\sin\gamma\cos\delta - \cos\gamma\cos\chi\sin\delta) \tag{4}$$

$$\dot{\gamma} = \left(\frac{V}{R} - \frac{g_R}{V}\right)\cos\gamma - \frac{g_\phi\sin\gamma\cos\chi}{V} + \frac{L}{Vm} + 2\Omega\sin\chi\cos\delta + \frac{\Omega^2 R\cos\delta(\cos\gamma\cos\delta + \sin\gamma\cos\chi\sin\delta)}{V} \tag{5}$$

$$\dot{\chi} = \frac{V\cos\gamma\sin\chi\tan\delta}{R} + \frac{F_y}{mV\cos\gamma} - 2\Omega(\tan\gamma\cos\chi\cos\delta - \sin\delta) + \frac{\Omega^2 r\sin\chi\cos\delta\sin\delta}{V\cos\gamma} - \frac{g_\phi\sin\chi}{V\cos\gamma} \tag{6}$$

The coordinate transformation between the Earth-fixed and geocentric inertial frames is given by the following equations:

$$\lambda^* = \lambda + \Omega t \tag{7}$$

$$\delta^* = \delta \tag{8}$$

$$R^* = R \tag{9}$$

$$V^*\sin\gamma^* = V\sin\gamma \tag{10}$$

$$V^*\cos\gamma^*\cos\chi^* = V\cos\gamma\cos\chi \tag{11}$$

$$V^*\cos\gamma^*\sin\chi^* = V\cos\gamma\sin\chi + \Omega R\cos\delta \tag{12}$$

Although the traditional entry trajectory analysis [9,10] neither accounts for the body attitude kinematics nor rotational dynamics, the present method requires both to predict the instantaneous, local flow angles for aerothermal load prediction. For the body attitude, a

quaternion-based formulation is undertaken to preclude the possibility of singularities at a pitch angle of 90 deg, which is otherwise a problem with the Euler-angle formulation. The kinematical equations of rotational motion in the body-fixed frame are as follows [8]:

$$\dot{q}_0 = -0.5(q_1 p + q_2 q + q_3 r) \tag{13}$$

$$\dot{q}_1 = 0.5(q_0 p + q_2 r - q_3 q) \tag{14}$$

$$\dot{q}_2 = 0.5(q_0 q + q_3 p - q_1 r) \tag{15}$$

$$\dot{q}_3 = 0.5(q_0 r + q_1 q - q_2 p) \tag{16}$$

$$q_0^2 + q_1^2 + q_2^2 + q_3^2 = 1 \tag{17}$$

The kinetic equations of rigid-body rotational motion in the body-fixed frame are the following:

$$\dot{\boldsymbol{\omega}} = \mathbf{J}^{-1}[\boldsymbol{\tau} - \mathbf{S}(\boldsymbol{\omega})\mathbf{J}\boldsymbol{\omega}] \tag{18}$$

where $\boldsymbol{\omega} = (p, q, r)^T$ is the angular velocity and

$$\mathbf{S}(\boldsymbol{\omega}) = \begin{bmatrix} 0 & -r & q \\ r & 0 & -p \\ -q & p & 0 \end{bmatrix} \tag{19}$$

The atmospheric model employed in this study is the 21-layer, 1976 U.S. Standard Atmosphere, which covers a geometric altitude range of 0–2000 km. The gravity model accounts for Earth's oblateness as well as zonal terms, resulting in the following radial and tangential components of acceleration due to gravity [8]:

$$g_R = \frac{GM_e}{R^2}\left[1 - \frac{3}{2}J_2\left(\frac{R_e}{R}\right)^2(3 - \cos^2\phi - 1) - 2J_3\left(\frac{R_e}{R}\right)^3\cos\phi(5\cos^2\phi - 3) - \frac{5}{8}J_4\left(\frac{R_e}{R}\right)^4(35\cos^4\phi - 30\cos^2\phi + 3)\right] \tag{20}$$

$$g_\phi = \frac{3GM_e}{R^2}\left(\frac{R_e}{R}\right)^2\sin\phi\cos\phi\left[J_2 + \frac{1}{2}J_3\left(\frac{R_e}{R}\right)\sec\phi(5\cos^2\phi - 1) + \frac{5}{4}J_4\left(\frac{R_e}{R}\right)^2(7\cos^2\phi - 1)\right] \tag{21}$$

where $\phi = (\pi/2) - \delta$ (the colatitude), R_e is the equatorial radius, and M_e is Earth's mass.

Aerothermodynamic Model

The entry object's profile is developed using three- or four-sided, elemental flat panels. As long as the body is convex with respect to the freestream, the assumption of a collisionless nature of the reflected particles is valid in the rarefied case, and a Newtonian/stagnation boundary-layer approximation can be used for the continuum case. The flowfield is numerically classified on the basis of Knudsen number Kn into free-molecular ($Kn > 10$), the transition ($0.01 \le Kn < 10$), and the continuum regimes ($Kn < 0.01$). For each body panel, the effective velocity used in flowfield calculations is a vector sum of the freestream velocity and the rotational velocity in a body frame:

$$\mathbf{v}_i = \mathbf{v}_\infty + \boldsymbol{\omega} \times \boldsymbol{\rho}_i \tag{22}$$

In the free-molecular regime, the forces and moments are calculated on the assumption of diffuse reflection of particles following a Maxwellian velocity distribution. The thermal, normal momentum, and tangential momentum accommodation coefficients are assumed to be unity for most engineering surfaces interacting with air, resulting in the following relations for the shear stress coefficient, pressure coefficient, and convective heat flux, respectively, on an elemental panel inclined at angle Θ to the effective flow [11]:

$$C_\tau s^2 = \frac{s\cos\Theta}{\sqrt{\pi}}\{e^{-s^2\sin^2\Theta} + \sqrt{\pi}s\sin\Theta[1 + \mathrm{erf}(s\sin\Theta)]\} \tag{23}$$

$$C_p s^2 = \left[\frac{s\sin\Theta}{\sqrt{\pi}} + \frac{1}{2}\sqrt{\frac{T_W}{T_\infty}}\right]e^{-s^2\sin^2\Theta} + \left[\left(\frac{1}{2} + s^2\sin^2\Theta\right) + \frac{1}{2}\sqrt{\frac{T_W}{T_\infty}}\pi s\sin\Theta\right][1 + \mathrm{erf}(s\sin\Theta)] \tag{24}$$

$$\frac{\dot{Q}}{\rho_\infty (c')^3} = \left(\frac{1}{4\sqrt{\pi}}\right)\left[\left(s^2 + \frac{\tilde{\gamma}}{\tilde{\gamma} - 1} - \frac{\tilde{\gamma} + 1}{2(\tilde{\gamma} - 1)}\frac{T_W}{T_\infty}\right)\{e^{-s^2\sin^2\Theta} + \sqrt{\pi}s\sin\Theta(1 + \mathrm{erf}[s\sin\Theta])\} - 0.5e^{-s^2\sin^2\Theta}\right] \tag{25}$$

For continuum hypersonic flow, modified Newtonian theory is used for pressure coefficient, and the following modification of Van Driest's [12] correlation of Lees-Dorodnitsyn laminar boundary-layer solution for a spherical stagnation region is employed for convective heat flux at the wall:

$$\dot{Q} = 0.763 Pr^{-0.6}\sqrt{\rho_e \mu_e}\sqrt{\frac{\mathrm{d}u_e}{\mathrm{d}x}}(h_{\mathrm{aw}} - h_w)\sin\Theta \qquad 20 \le \Theta \le 160\,\mathrm{deg} \tag{26}$$

where Pr is Prandtl number (assumed constant at 0.715 for perfect air),

$$\frac{\mathrm{d}u_e}{\mathrm{d}x} = \frac{1}{r_n}\sqrt{\frac{2(p_e - p_\infty)}{\rho_e}} \tag{27}$$

is the Newtonian velocity gradient with stagnation region radius r_n, and the difference between adiabatic wall enthalpy and wall enthalpy is computed using the recovery factor $\sqrt{Pr}$ as follows:

$$h_{\mathrm{aw}} - h_w = \sqrt{Pr}(h_0 - h_e) = c_p\sqrt{Pr}(T_0 - T_e) \tag{28}$$

Here c_p is the constant pressure specific heat, and T_0 is the stagnation temperature. The boundary-layer edge quantities (denoted by subscript e) for the stagnation region are obtained using Rankine–Hugoniot normal shock relations, and the viscosity coefficient is calculated from Sutherland's law. For a windward panel with flow deflection smaller than 20 deg (or larger than 160 deg), the heat flux obtained from Eq. (26) with $\Theta = 20$ deg is used.

In the case of transition flow, a logarithmic interpolation with respect to the Knudsen number is employed as a bridging relation (cf. Koppenwallner and Legge [7]) between the aerothermal quantities calculated for the free-molecular flow (subscript FM) and the continuum hypersonic flow (subscript N) regimes, e.g., the following expression for heat flux:

$$\dot{Q} = \dot{Q}_N + \frac{1}{3}(\dot{Q}_{\mathrm{FM}} - \dot{Q}_N)[\log_{10}(Kn) + 2], \qquad 0.01 \le Kn \le 10 \tag{29}$$

Finally, the aerodynamic forces and moments on the body can be evaluated by summing over the elemental flat panels as follows:

$$\frac{\mathbf{f}}{q_\infty A} = \sum_{i=1}^{N} \{C_{p_i}(-\hat{\mathbf{n}}_i) + C_{\tau_i}[\hat{\mathbf{n}}_i \times (\hat{\mathbf{v}}_i \times \hat{\mathbf{n}}_i)]\} \tag{30}$$

$$\frac{\boldsymbol{\tau}}{q_\infty A c} = \sum_{i=1}^{N} (\boldsymbol{\rho}_i \times \{C_{p_i}(-\hat{\mathbf{n}}_i) + C_{\tau_i}[\hat{\mathbf{n}}_i \times (\hat{\mathbf{v}}_i \times \hat{\mathbf{n}}_i)]\}) \tag{31}$$

Thermomechanical Breakup Model

A methodology to predict aerothermal breakup is necessary to model the subsequent tracks of disintegrated debris. A complete and accurate prediction of aerothermal breakup requires the following steps: 1) 6 degree-of-freedom flight model to predict trajectory and attitude, 2) aerodynamic analysis to compute perturbing forces and moments, 3) aerothermal analysis to determine heat flux, 4) thermal analysis to determine heat balance in each part of the reentry object, and 5) a structural analysis to monitor local stress levels.

The present method incorporates steps 1–3, whereas 4 and 5 require an altogether different expertise, based on material and structural properties, and are beyond the present scope. However, one can define cutplanes along which breakup is expected to happen, and then use steps 1–3 for estimating heat flux distribution on the newly created objects, which in turn may cause further breakup along new cutplanes. The definition of a cutplane is crucial to the study and can be based on either a predefined joint (such a lines of rivets/bolts/welds), or a general semi-empirical thermomechanical stress parameter obtained by combining thermal flux on a panel and its centrifugal stress level.

Evaluation of Cutplanes

A cutplane is defined by the three most thermally stressed points on the object's surface, which are selected by surveying all the surface panels. Total stress magnitude on a surface panel can be assumed to be directly proportional to the surface heating rate (heat flux multiplied by area). When the surface fluxes of two panels are the same, the panel with a larger centrifugal acceleration at its centroid will have a larger stress level. Because it is also logical to assume that fragmentation would occur along points that are the most highly stressed, a governing stress parameter has been proposed as the product of the heating rate and centrifugal acceleration. A survey is thus conducted of the following thermomechanical stress parameter obtained by multiplying the thermal flux $\dot{Q}$ with the centrifugal acceleration magnitude $a_N = |\boldsymbol{\omega} \times (\boldsymbol{\omega} \times \boldsymbol{\rho}_i)|$ on the ith panel of area A_i:

$$G_i = A_i \dot{Q} |\boldsymbol{\omega} \times (\boldsymbol{\omega} \times \boldsymbol{\rho}_i)| \tag{32}$$

The shape of resulting debris fragments depends on how each panel of the original object is intersected by the cutplane. There are three distinct ways in which a quadrilateral panel can be cut. Similarly, the common base plane must be subdivided into new quadrilateral panels. Identification of the cut method and the calculation of coordinates of the new panel corners is a major coding task that requires much time and effort. The resulting geometry module is a self-adaptive scheme that can generate debris fragments from any given shape. Figure 1 shows an example of cutting an entry capsule into two unequal fragments by a cutplane passing through the points (−0.5, 0.1, −1), (0.3, 0.5, 0), and (0.5, −0.1, −0.2).

When the thermal gradient at any point on the cutplane exceeds a reference magnitude $\dot{Q}_R$, it is assumed that the critical aerothermal stress on that part has been reached and the cut is performed. In this manner, a reasonable breakup profile along the trajectory is achieved. The aerothermal breakup estimate includes complete ablation, in which some debris fragments are totally melted. If the fragment volume is less than a critical value, and the surface flux is greater than the melting heat flux, it is assumed that the fragment will be completely ablated. Such a model is logical, because the net temperature increases with heat influx and decreases with an increasing total volume. Another criteria for fragmentation is the maximum centrifugal acceleration, $(a_N)_{\max} = |\boldsymbol{\omega} \times (\boldsymbol{\omega} \times \boldsymbol{\rho}_i)|_{\max}$, which, if exceeds a reference magnitude a_R, is assumed to result in complete mechanical disintegration, causing a shower of small debris fragments. After each breakup, the surviving debris fragments' trajectories are simulated until either impact or subsequent disintegration/complete ablation. Therefore, the scheme accounts for an indefinite number of separate trajectories following breakup events.

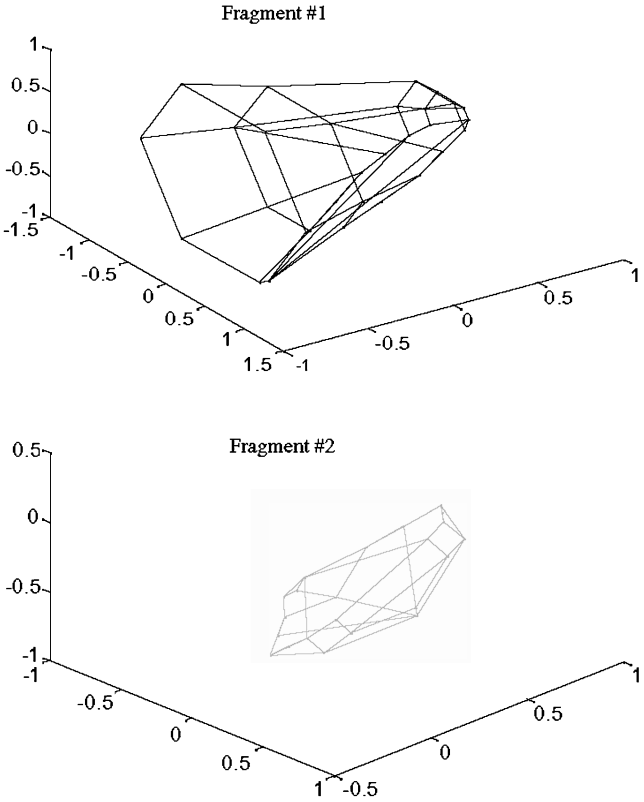

Fig. 1 Fragments resulting from a sample breakup by cutplane (all axes in meters).

Inertia Module

It is necessary to establish inertial properties of each debris fragment after a breakup event. To do so, a shell-like structure with lumped masses and an average structural thickness are assumed. As soon as a debris fragment is created, its mass and inertia tensors are computed based on the new panel coordinates using a dedicated inertia module.

Breakup Model and Trajectory Simulation Algorithm

The breakup modeling sequence and its incorporation in trajectory simulation can be described by the algorithm depicted in Fig. 2. It is to be noted that tracking of debris fragments depends on the identification of the largest parent fragment at each instant, as well as the predefined duration t_s, for which the fragments are individually tracked. The iteration over debris fragments includes complete thermal ablation and mechanical disintegration by centrifugal stresses. Consequently, the surviving debris fragments may continually lose mass until ground impact or until complete ablation/disintegration. As soon as a fragment meets the criterion of complete ablation or mechanical disintegration, its state vector is frozen and its trajectory is not simulated further. Thus, there is no attempt to model how long a fragment takes to melt, or to produce a debris shower, and what happens to its trajectory in the meantime. As soon as new debris is generated, its state vector and geometry are fed back to the dynamics and aerothermal loads modules, and simulation is performed over the next time interval. Only the largest surviving

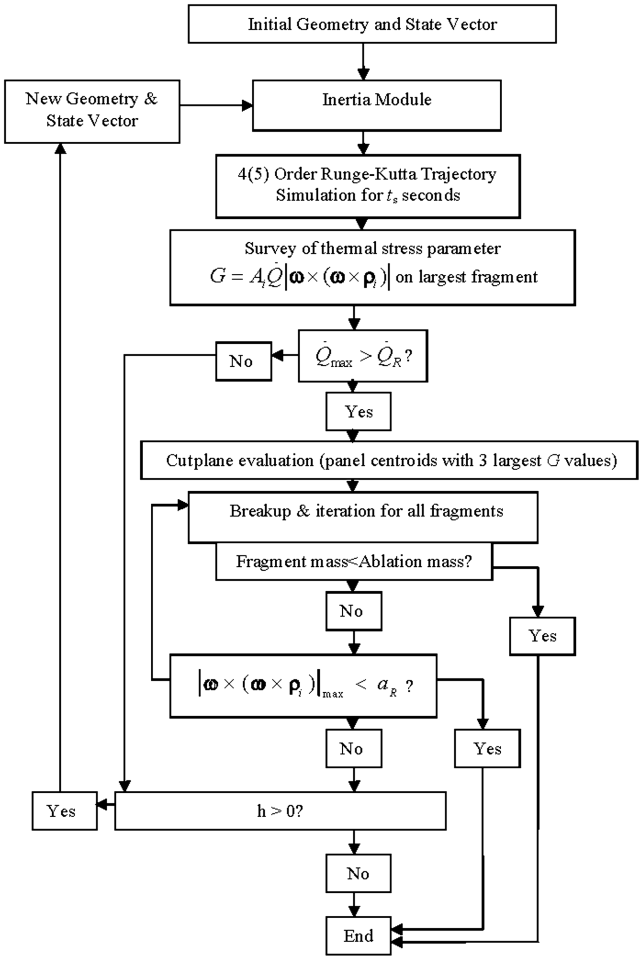

Fig. 2 Flowchart for entry trajectory simulation with aerothermal breakup.

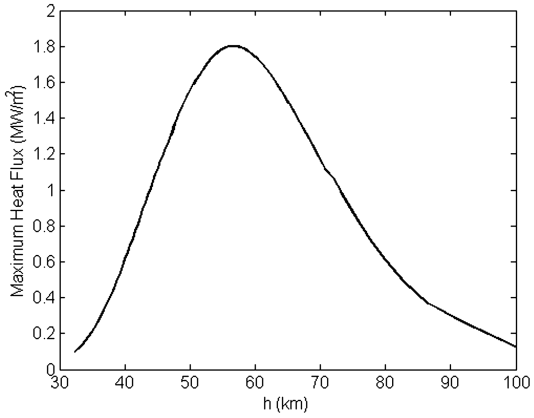

Fig. 3 Maximum heat flux of entry capsule with nominal trajectory without breakup.

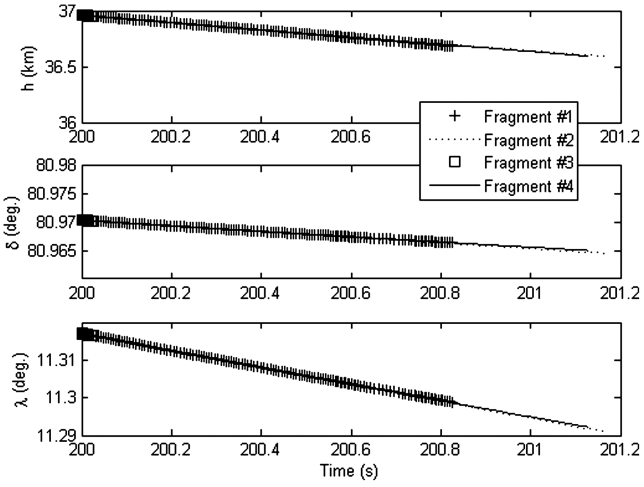

Fig. 4 Altitude and ground track during simulated breakup.

fragment is tracked for long-term simulation, whereas the other fragments are tracked only for duration t_s. When a fragment is either completely ablated/disintegrated or reaches ground level, its simulation is ended. Hence, the scheme results in a complete simulation of the entry trajectory with en route debris shedding events until either ground impact or complete ablation and mechanical disintegration.

Numerical Results

We begin the trajectory simulation using a preliminary tracking of the four largest fragments resulting from a breakup event of an entry capsule at $t = 200$ s. The capsule is a flared sphere cone with nose radius 0.32 m, initial cone semi-angle 22.78 deg and length 0.8 m, final cone semi-angle 28.31 deg and length 0.445 m, and base diameter 2.13 m. Its mass is 423 kg, with principal moments of inertia 236.38, 240.74, and 272.93 kg $\cdot$ m^2, respectively, and reference length is 1.557 m. The nominal entry trajectory is specified in Table 1, and the computed heat flux for the nominal (unbroken) case is shown in Fig. 3. The disturbance to nominal entry is assumed to be caused by an initial flow perturbation at entry due to initial angular velocity $\boldsymbol{\omega}(0) = (0, 0.0087, -0.0087)^T$ deg/s and initial quaternion $q_0(0) = 0.9998$, $q_1(0) = 7.75 \times 10^{-6}$, $q_2(0) = 0.0183$, and $q_3(0) = -4.235 \times 10^{-4}$. The simulated breakup trajectory is shown in Figs. 4–6. A scatter of the fragments is evident in Fig. 4, with increased velocity deviation (Fig. 5) caused by high body rates (Fig. 6) of the aerodynamically unstable fragments. The high body rates encountered by the smaller fragments are likely to cause their further disintegration, and the fragments are unlikely to survive reentry. However, detailed thermomechanical disintegration of fragments is included in the following study.

Detailed Simulation with Thermomechanical Fragmentation

We now consider detailed simulation with aerothermal breakup, ablation, and mechanical disintegration of the previously described entry capsule from its given initial trajectory (Table 1). For this object with an ablative heat shield, a reference heat flux of $\dot{Q}_R = 1.2$ MW/m^2 is taken for defining the cutplane, and a melting surface flux of 1.5 MW/m^2 is taken for complete ablation of a fragment of volume less than 0.1 m^3. For complete mechanical disintegration of a fragment, a limiting reference centrifugal acceleration of $a_R = 225$ m/s^2 $(23g)$ is assumed. The acceleration, thermal flux, and stress parameter distributions on the vehicle 101 s after entry are shown in Table 2. This is the point in the nominal trajectory when the

Table 1 Unbroken object's nominal trajectory

h, km	δ, deg	λ, deg	V, km/s	γ, deg	χ, deg
648.02	44.487	259.521	7.342667 (inertial)	−0.809 (inertial)	101.103 (inertial)
100.00	23.471	83.5785	7.966280 (inertial), 8.042530 (relative)	−2.3126 (inertial), −2.2907 (relative)	261.388 (inertial), 258.332 (relative)
5.00	10.4284	80.7862	0.46585 (inertial), 0.085725 (relative)	−10.604 (inertial), −89.915 (relative)	359.9925 (inertial), 331.916 (relative)

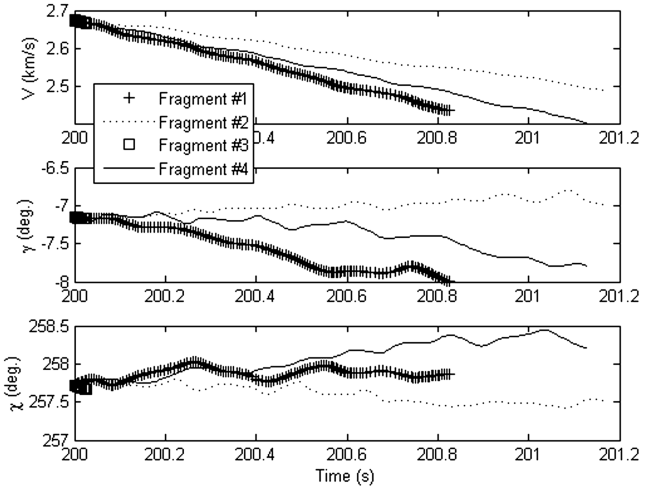

Fig. 5 Velocity vector coordinates during simulated breakup.

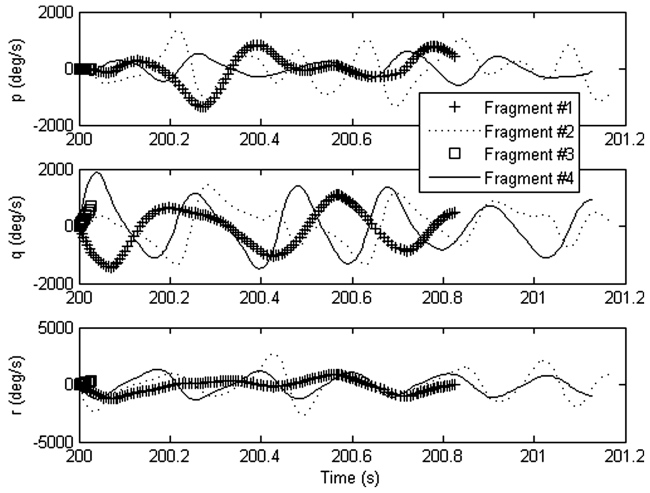

Fig. 6 Body rates during simulated breakup.

reference heat flux is first exceeded, resulting in aerothermal breakup and debris generation. Each surviving debris fragment is simulated for $t_s = 1$ s, and the important state variables are plotted in Figs. 7–9. Constant tracks in these plots indicate frozen values of the state

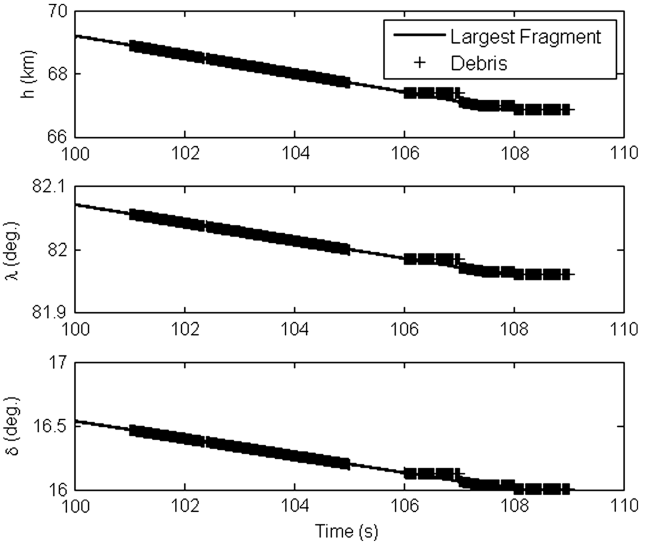

Fig. 7 Altitude profile and ground track with aerothermal breakup.

vector if either mechanical disintegration or complete ablation criterion is met at any time during the simulation. Note that the largest fragment disintegrates at $t = 109$ s, therefore, the vehicle does not survive below an altitude of about 67 km. The debris shower is limited to within 0.46 deg of latitude and 0.1 deg of longitude, resulting in a total impact ground track of about 52.4 km, roughly ending at latitude 16 deg and longitude 82 deg. The large body rates due to an unstable aerodynamic configuration after breakup often cause rapid mechanical disintegration by high centrifugal stresses (Fig. 10). Hence, all debris is either completely disintegrated or ablated within 8 s of the initial breakup event. Table 3 tracks the mass of the largest surviving fragments following individual breakup events.

Dispersion Analysis and Risk Estimates

Parametric studies are conducted next, consisting of variations in the initial conditions at reentry (debris orbital parameters) and their effects on the final debris field. It is expected that, from these numerical studies, one may evolve a risk estimate for impacting debris in a particular region. Estimation of risk is in the form of dispersion analysis for range deviations, beginning from the nominal entry trajectory. There is no change in the limiting values of

Table 2 Acceleration, thermal flux and stress parameter distribution over surface panels at 101 s after entry

ρ_i, m			a_N, m/s^2	$\dot{Q}$, $\times 10^6$ W/m^2	G_i, $\times 10^6$ W · m/s^2
0.2132	−0.7126	−0.4114	0.7312	0.4963	0.3629
0.2132	−0.0000	−0.8228	1.2786	0.3551	0.4541
0.2132	0.7125	−0.4114	0.9428	0.3745	0.3531
0.2132	0.7126	0.4114	0.7983	0.5351	0.4272
0.2132	0.0000	0.8228	1.2838	0.6765	0.8685
0.2132	−0.7126	0.4114	0.8942	0.6571	0.5875
0.8125	−0.5032	−0.2905	0.3883	0.3972	0.1542
0.8125	−0.0000	−0.5809	0.8166	0.2510	0.2050
0.8125	0.5032	−0.2905	0.5077	0.2708	0.1375
0.8125	0.5032	0.2905	0.3571	0.4373	0.1562
0.8125	0.0000	0.5809	0.8148	0.5838	0.4756
0.8125	−0.5032	0.2905	0.5273	0.5637	0.2972
1.2920	−0.3111	−0.1795	0.8956	0.9935	0.8898
1.2920	0	−0.3591	0.9881	0.9049	0.8941
1.2920	0.3111	−0.1795	0.8908	0.9173	0.8171
1.2920	0.3111	0.1795	0.8605	1.0177	0.8757
1.2920	0	0.3591	0.9840	1.1057	1.0881
1.2920	−0.3111	0.1795	0.9205	1.0939	1.0069
1.3413	−0.1107	0.1917	0.9696	1.2205	1.1833
1.3413	0	0	0.9238	1.2203	1.1274
1.3413	−0.1107	0.1917	0.9696	1.2205	1.1833

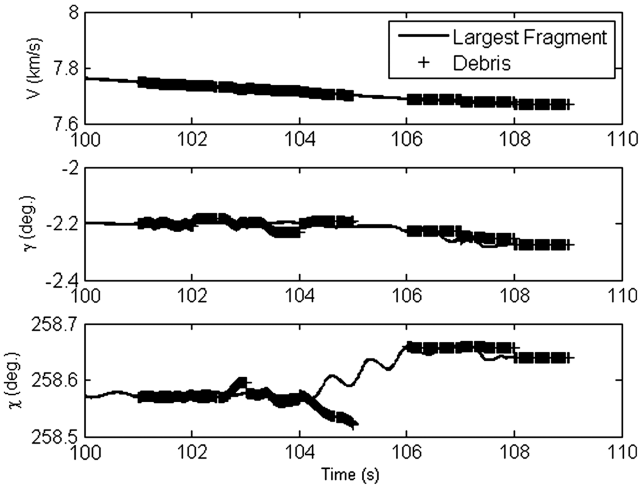

Fig. 8 Velocity vector coordinates with aerothermal breakup.

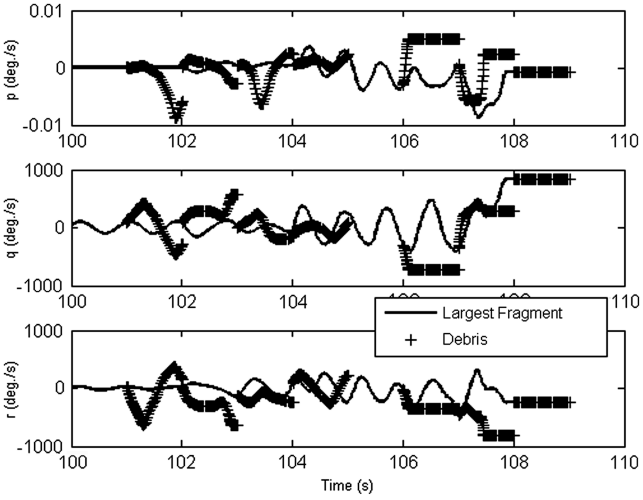

Fig. 9 Body rates during aerothermal breakup.

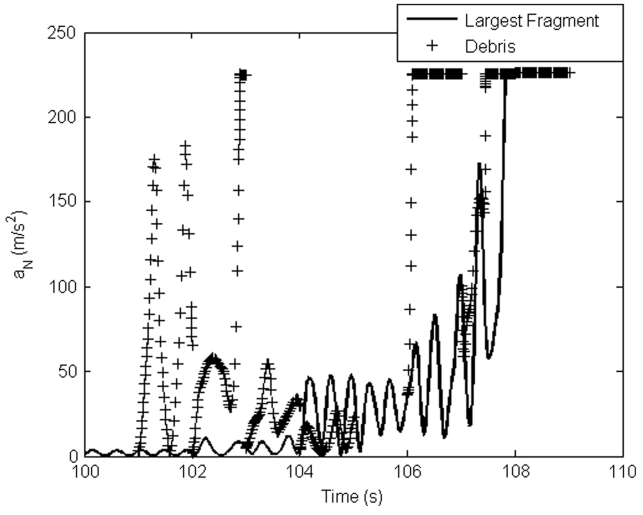

Fig. 10 Centrifugal acceleration magnitude with aerothermal breakup.

Table 3 Largest surviving fragment

Largest fragment no.	Time of creation, s	Initial mass, kg
1	0	423
2	101	359.23
3	102	260.91
4	103	244.93
5	104	197.99
6	106	169.20
7	107	145.98
8	108	136.39

maximum allowable heat flux and centrifugal acceleration from those considered earlier. A $\pm 10\%$ deviation in the speed, flight-path angle, heading angle, and mass at entry from the nominal condition of Table 1 is considered, and the first breakup event, the final debris fragment, and the downrange spread of intermediate debris are tabulated in Table 4. Increases in entry speed, flight-path angle, and heading angle are seen to have the largest influence on the debris field length, as well as final altitude. The speed and flight-path angle have the greatest influence on the downrange dispersion, whereas the heading-angle variation causes the largest cross-range dispersion. Increase in the object's entry mass (assumed nominally distributed) has a negligible effect on the debris field, although a 10% decrease in the mass causes an appreciable variation. The apparent reason for this is that there is little change in the altitude of critical thermal loading (and hence the time of the first breakup) when the mass is increased. However, a reduction in the mass hastens thermomechanical breakup as the critical load is reached earlier in the trajectory.

If a risk estimate of impacting debris is to be obtained within a specified region (perhaps defined by an impact ellipse), a careful study of likely parametric variations must be conducted, such as that presented in Table 4. For example, an object entering from an elliptical orbit has the largest probable variation in the entry velocity vector (speed, flight-path, and heading angles), which (according to Table 4) is likely to have a $\pm 100\%$ dispersion in both downrange and cross-range extent of the nominal debris field. In simple terms, it could be stated that the risk probability of off-nominal impact increases by as much as 100%, even if there is only a 10% variation in the orbital parameters. A more accurate risk estimate can be obtained by precisely determining the entry condition dispersion caused by likely variations in the orbital parameters.

Conclusions

The procedure for modeling the reentry trajectory of space debris, incorporating an accurate flow model and complete vehicle dynamics, is found to be a reasonable method for atmospheric breakup and debris generation. Breakup modeling is based on thermal flux and centrifugal acceleration patterns on the object surface, thereby producing a most probable cutplane. Hence, the scheme results in a complete simulation of the entry trajectory with en route debris shedding events until either ground impact or complete ablation and mechanical disintegration. An entry capsule with initially stable aerodynamic configuration is selected for the trajectory simulations. An entry condition representative of deboost from a circular or elliptical orbit is considered. With the specified aerothermal limits, the capsule is found to disintegrate completely within a few minutes of entry, causing a shower of small debris fragments. The observed fragmentation, debris field estimate, and its dispersion due to orbital parametric variations all crucially depend on the reference heat flux and centrifugal acceleration magnitudes assumed in the analysis. Although the numbers assumed for a_R and $\dot{Q}_R$ in the present study are only rough estimates, they offer an insight into the trajectory sensitivity to material and structural properties. For a faithful trajectory model with aerothermal breakup, a careful predetermination of the limiting aerothermal loads is required, perhaps based either on experimental data or a thermomechanical stress analysis including structural and material properties. Such a study is usually a part of detailed vehicle design and prototype structural testing.

Table 4 Dispersion in the debris field due to parametric variation at entry

Parameter	Time of first breakup, s	Time of last debris, s	Altitude of first breakup, km	Altitude of last debris, km	Latitude of first breakup, deg	Latitude of last debris, deg	Longitude of first breakup, deg	Longitude of last debris, deg	Length of debris field, km	Midpoint of debris field, lat/long, deg
Nominal	101	109	68.89	66.86	16.47	16.01	82.06	81.96	52.4	16.24/82.01
(+)10% V	137	148	72.40	71.62	13.09	12.30	81.41	81.25	89.7	12.695/81.33
(−)10% V	99	111	63.70	59.38	17.30	16.70	82.19	82.06	68.3	17.0/82.125
(+)10% $\lvert\gamma\rvert$	91	98	68.97	67.25	17.16	16.80	82.20	82.13	40.8	16.98/82.165
(−)10% $\lvert\gamma\rvert$	116	125	68.15	66.09	15.44	14.94	81.84	81.74	56.8	15.19/81.79
(+)10% $\lvert\chi\rvert$	97	102	70.08	68.93	17.40	17.16	79.89	79.75	30.9	17.28/79.82
(−)10% $\lvert\chi\rvert$	105	113	67.71	65.65	16.23	15.78	84.50	84.56	50.5	16.005/84.53
(+)10% m	101	109	68.91	66.70	16.46	15.96	82.06	81.95	57.0	16.21/82.005
(−)10% m	102	112	68.59	65.66	16.41	15.74	82.04	81.90	76.2	16.075/81.97

Acknowledgments

This study was supported in part by a research grant from the Indian Space Research Organization. The author is grateful to G. Koppenwallner for reviewing this paper.

References

[1] Koppenwallner, G., Fritsche, B., Lips, T., Martin, T., Francillout, L., and De Pasquale, E., "Analysis of ATV Destructive Re-Entry Including Explosion Events," *4th European Conference on Space Debris*, SP-587, ESA Noordwijk, The Netherlands, Aug. 2005, pp. 545–550.

[2] Mendeck, G. F., and Kadwa, B., "Public Life Risk Assessment of Off-Nominal Genesis Entries," *Advances in Astronautical Sciences*, Vol. 120 II, American Astronautical Society, San Diego, CA, 2005, pp. 1923–1938.

[3] Larson, E. W. F., Haber, J. M., Morris, J. O., and Collins, J. D., "A General Methodology for Analysis of Risks from Falling Debris," *1st IAASS Conference*, SP-599, ESA Noordwijk, The Netherlands, Aug. 2005, pp. 125–130.

[4] Koppenwallner, G., Fritsche, B., and Lips, T., "Survivability and Ground Risk Potential of Screws and Bolts of Disintegrating Spacecraft During Uncontrolled Re-Entry," *Proceedings of the 3rd European Space Debris Conference*, ESA SP-473, 2001, pp. 533–539.

[5] Lips, T., Fritsche, B., Koppenwallner, G., and Klinkrad, H., "Spacecraft Destruction During Re-Entry: Latest Results and Development of the SCARAB Software System," *Advances in Space Research*, Vol. 34, No. 5, 2004, pp. 1055–1060. doi:10.1016/j.asr.2003.01.012

[6] Lips, T., Wartemann, V., Koppenwallner, G., Klinkrad, H., Alwes, D., Dobarco-Otero, J., Smith, R. N., DeLaune, R. M., Rochelle, W. C., and Johnson, N. L., "Comparison of ORSAT and SCARAB Reentry Survival Results," *4th European Conference on Space Debris*, SP-587, ESA Noordwijk, The Netherlands, Dec. 2005, pp. 533–538.

[7] Koppenwallner, G., and Legge, H., "Drag of Bodies in Rarefied Hypersonic Flow," *Thermophysical Aspects of Re-Entry Flows*, Vol. 103, edited by C. D. Scott and J. N. Moss, Progress in Astronautics and Aeronautics, AIAA, Washington, D.C., 1994, pp. 44–59.

[8] Tewari, A., *Atmospheric and Space Flight Dynamics-Modeling and Simulation*, Birkhäuser, Boston, 2006.

[9] Chapman, D. R., "An Approximate Analytical Method for Studying Entry into Planetary Atmospheres," NASA TR R-11, 1959.

[10] Loh, W. H. T., *Dynamics and Thermodynamics of Planetary Entry*, Prentice–Hall, Englewood Cliffs, NJ, 1963.

[11] Schaaf, S. A. and Chambre, P. L., "Flow of Rarefied Gases," *High-Speed Aerodynamics and Jet Propulsion*, Vol. 3, edited by H. W. Emmons, Fundamentals of Gas Dynamics, Princeton Univ. Press, Princeton, NJ, 1958, pp. 687–739.

[12] Van Driest, E. R., "The Problem of Aerodynamic Heating," *Aeronautical Engineering Review*, Oct. 1956, pp. 26–41.

A. Ketsdever
Associate Editor